

# Random-walk shielding-potential viscosity model for warm dense metals

Yuqing Cheng,<sup>1,2</sup> Haifeng Liu,<sup>2, a)</sup> Yong Hou,<sup>3</sup> Xujun Meng,<sup>2</sup> Qiong Li,<sup>2</sup> Yu Liu,<sup>2</sup> Xingyu Gao,<sup>2</sup> Jianmin Yuan,<sup>4</sup> Haifeng Song,<sup>2</sup> and Jianguo Wang<sup>2</sup>

<sup>1)</sup>*School of Mathematics and Physics, University of Science and Technology Beijing, Beijing 100083, China*

<sup>2)</sup>*Laboratory of Computational Physics, Institute of Applied Physics and Computational Mathematics, Beijing 100094, China*

<sup>3)</sup>*Department of Physics, College of Liberal Arts and Sciences, National University of Defense Technology, Changsha 410073, China*

<sup>4)</sup>*Graduate School, China Academy of Engineering Physics, Beijing 100193, China*

(Dated: 14 September 2021)

The collective effect on the viscosity is essential for warm dense metals. The statistics of random-walk ions and the Debye shielding effect describing the collective properties are introduced in the random-walk shielding-potential viscosity model (RWSP-VM). As a test, the viscosities of several metals (Be, Al, Fe and U) are obtained, which cover from low-Z to high-Z elements. The results indicate that RWSP-VM is a universal accurate and highly efficient model for calculating the viscosity of metals in warm dense state.

## I. INTRODUCTION

The transport properties of matters have been widely investigated. In particular, the shear viscosity is crucial for the inertial confinement fusion (ICF) capsules<sup>1</sup>, understanding wave damping in dense plasmas<sup>2</sup>, microjetting during shock-loaded<sup>3</sup> and understanding the evolution of astrophysical objects<sup>4</sup>. The measurements of viscosity have been conducted at a pressure near 1 bar, while it is very difficult to implement at high temperature and high pressure<sup>5,6</sup>. Researchers have been investigating the viscosity by employing three different kinds of methods. Firstly, Alfè and Gillan<sup>7</sup> employed the quantum molecular dynamics (QMD) based on first principles and molecular dynamics (MD) simulations to calculate the viscosity of liquid Al and Fe-S using the Green-Kubo relations<sup>8</sup>, and some of the authors (H. Liu and H. Song) have studied the viscosity of liquid Al and Pu in the previous work by the similar method<sup>9,10</sup>, the time step and simulation length of which are several fs and dozens of ps up to 100 ps, respectively. However, the number of bands which ensures the accuracy of the simulation increases rapidly with the increasing temperature for warm dense matters, which contain partially ionized electrons that interact strongly with the nuclei. Thereby, the expensive overhead of full QMD simulation for viscosity makes it difficult to obtain enough data. Secondly, some of the authors (Y. Hou and J. Yuan) developed the average-atom model combined with the hyper-netted chain (AAHNC) approximation as an efficient tool to calculate electronic and ionic structure<sup>11</sup>. The viscosity of Al is calculated by using both Langevin MD (LMD) and classical MD (CMD) simulations, and the results agree well with the results of the orbital-free MD (OFMD), quantum orbital-free MD (QOFMD), the effective potential theory + average

atom (EPT+AA) and pseudo-atom MD (PAMD) in Ref. 12 and 13. Nevertheless, the efficiency is still low when employing these methods because of the high computational cost, especially at high temperatures and high pressures, which will limit their applications. Thirdly, some researchers have developed models to calculate the viscosity<sup>14,15</sup>. Daligault et al. develop the one-component plasma (OCP) model that is based on equilibrium MD simulations and the Green-Kubo relation<sup>8</sup> to evaluate the viscosity of one-component matters from the weakly-coupled regime to solidification threshold, with a practical formula provided<sup>14</sup>. Murillo proposes a practical model to compute the viscosity of liquid metals over wide ranges, which is based on the Yukawa model and the MD data in the range of interest<sup>15</sup>. However, these semiempirical models include some fitting parameters without any physical significance. The validate region of these models is limited to the simulations, which hinders the applications.

In this study, we develop a new model called the random-walk shielding-potential viscosity model (RWSP-VM) for the viscosity of metal elements at warm dense state. The quantitative comparison studies of several methods on a series of metal elements show that RWSP-VM is a universal, accurate and highly efficient model for calculating the viscosity of metals in warm dense state.

## II. MODEL

For metals at warm dense state, the electrons are ionized partially and the velocities of the ions are very high. This indicates that these ions move as “ion gas” randomly with the Coulomb interactions between each other. Meanwhile, the Debye shielding effect caused by the numerous ionized electrons will weaken the Coulomb interactions. The random process of the ions could be treated employing the random-walk concept<sup>16</sup>. Here, on account of the random-walk “ion gas” and the Debye shielding effect, we make two assumptions.

<sup>a)</sup>Corresponding author: liu\_haifeng@iapcm.ac.cn

Assumption 1: Ions move randomly as “ion gas”, and only binary collisions of ions are considered for simplicity.

Assumption 2: There is a cut-off distance  $r_0$ , i.e., only when the distance  $r$  between a pair of ions is less than  $r_0$ , the Coulomb interaction works, resulting in the shielding-potential.

Here, the Coulomb interaction is described as  $\phi(r) = q^2/r$ , where  $q^2 = (Ze)^2/(4\pi\epsilon_0)$ ,  $Ze$  is the charge of the ion,  $e$  is the elementary charge, and  $\epsilon_0$  is the electric constant.

In the beginning, the definition of the shear viscosity  $\eta$  is described as<sup>8</sup>:

$$\eta = \frac{1}{2t} \frac{V}{k_B T} \langle (\mathcal{L}_{\alpha\beta}(t) - \mathcal{L}_{\alpha\beta}(0))^2 \rangle, \quad (1)$$

where  $t$  is the time,  $V$  is the volume of the system,  $k_B$  is the Boltzmann constant,  $T$  is the temperature,  $\langle \dots \rangle$  stands for the ensemble average and  $\mathcal{L}_{\alpha\beta} = \frac{1}{V} \sum_i r_{i\alpha} p_{i\beta}$ .

Here,  $\alpha$  and  $\beta$  stand for the directions in Cartesian coordinate with  $\alpha \neq \beta$ ;  $r_{i\alpha}$  and  $p_{i\beta}$  are the coordinate in  $\alpha$  direction and the momentum in  $\beta$  direction of the  $i$ -th ion, respectively. For simplicity, we set  $\alpha = x$ ,  $\beta = y$  and  $\mathcal{L}_{\alpha\beta}(0) = 0$ . Hence,

$$\langle (\mathcal{L}_{\alpha\beta}(t))^2 \rangle = \frac{m^2}{V^2} \sum_i (x_i v_{iy})^2 = \frac{m^2}{V^2} N \langle (x v_y)^2 \rangle. \quad (2)$$

Here,  $m$  is the mass of an ion,  $N$  is the total number of the ions and  $v_y$  is the velocity in  $y$  direction at time  $t$ . We can calculate the quantity  $\langle (x v_y)^2 \rangle$  by using the random-walk assumption (Assumption 1),

$$\langle (x v_y)^2 \rangle = \left[ \left( \sum_{j=1}^{N_s} \Delta x_j \right) \left( \sum_{j=1}^{N_s} \Delta v_{jy} \right) \right]^2. \quad (3)$$

Here,  $\Delta x_j$  and  $\Delta v_{jy}$  are the change of  $x$  and  $v_y$  of the  $j$ -th step walk of an ion, respectively, and  $N_s \approx \nu t$  is the total step within time  $t$ , where  $\nu = v/\lambda$  is the collision frequency and  $\lambda$  is the mean free path of the ions. Assumption 1 allows to reject the cross term of Eq. (3) when computing the ensemble average. Then we obtain:

$$\langle (x v_y)^2 \rangle = N_s \langle (\Delta x)^2 \rangle \langle (\Delta v_y)^2 \rangle = N_s \frac{2}{3} \lambda^2 \langle (\Delta v_y)^2 \rangle. \quad (4)$$

Here we use the relation  $\langle (\Delta x)^2 \rangle = \frac{2}{3} \lambda^2$ . So far, the problem turns to be the calculation of  $\langle (\Delta v_y)^2 \rangle$ .

Assumption 2 allows the trajectory of one ion to be hyperbolic curve when the pair distance is below the cut-off distance  $r_0$ , which is shown in Fig. 1. Ion A moves toward ion B. The hyperbolic equation is:

$$\frac{x^2}{a^2} - \frac{y^2}{b^2} = 1 \quad (x > 0, \quad c = \sqrt{a^2 + b^2}). \quad (5)$$

The parameter is  $a = \frac{q^2}{3k_B T + 2q^2/r_0}$  and  $b$  is an independent variable. Here,  $q^2 = \frac{(Ze)^2}{4\pi\epsilon_0}$ ,  $\overline{Z} = \frac{1}{n} \sum_{j=0}^{Z_{nc}} j n_j$

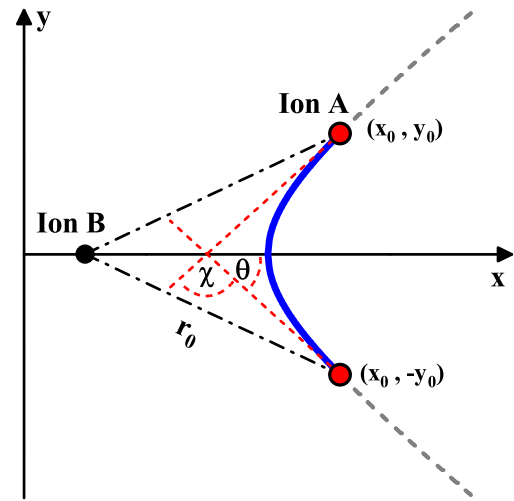


FIG. 1. Hyperbolic track (blue curve) of an ion for RWSP-VM.  $\chi$  is the angle variation of the ion's velocity during one “collision”.  $\theta$  is the angle between the initial velocity of the ion and the  $x$  axis.

is the average ionization,  $Z_{nc}$  is the nuclear charge, and  $n_j$  is the number density of the  $j$ -th ionized ions. The coordinate  $(x_0, y_0)$  is given as  $x_0 = \frac{a}{c}(r_0 - a)$ ,  $y_0 = \frac{b}{c} \sqrt{(r_0 - a)^2 - c^2}$ . Here, the maximum of  $b$  is  $b_m = \sqrt{r_0^2 - 2r_0 a}$ ,  $\tan \theta = \frac{x_0 b^2}{y_0 a^2}$  and the angular variation of the ion's velocity is  $\chi = \pi - 2\theta$ . Therefore, quantity  $\langle (\Delta v_y)^2 \rangle$  is

$$\langle (\Delta v_y)^2 \rangle = \int_0^{b_m} \frac{1}{\nu} 2\pi b v n (v \sin \chi)^2 db = \frac{2\pi v^3 n}{\nu} I(T), \quad (6)$$

where we define  $I(T) = \int_0^{b_m} b (\sin \chi)^2 db$  and  $n$  is the number density of the ions. By using the relations  $\nu = \sqrt{2\pi n d^2 v}$  and  $mv^2 = 3k_B T$ , the shear viscosity  $\eta$  can be expressed as follows:

$$\eta = \frac{\sqrt{3m k_B T}}{\pi d^4} I(T). \quad (7)$$

Here  $d$  is the collision diameter. For physical consideration, the parameters are set as  $r_0 = d$  and  $d = \lambda_D$ . Here,  $\lambda_D \equiv \sqrt{\frac{\epsilon_0 k_B T}{n_e e^2 (z^* + 1)}}$  is the Debye length,  $n_e$  is the number density of electrons and  $z^* \equiv \overline{Z^2}/\overline{Z}$ . For metals,  $\overline{Z^2} = \frac{1}{n} \sum_{j=0}^{Z_{nc}} j^2 n_j$ .

The viscosities of metal elements in warm dense range are calculated fastly from Eq. (7). Besides, in RWSP-VM, we only require several known and/or easily available input parameters of the ion (atom mass, nuclear charge, ionization, etc.) and some physical constants (electric constant, Boltzmann constant and elementary charge), making it different from other models.

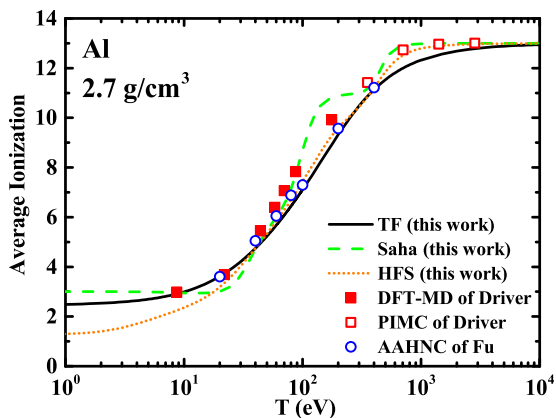


FIG. 2. Average ionization  $\bar{Z}$  of Al at the density of  $2.7 \text{ g/cm}^3$ . Black solid, green dashed and origin dot lines stand for the results of TF, Saha and HFS models, respectively. Red filled and open squares stand for DFT-MD and PIMC results of Driver<sup>18</sup>, respectively. Blue open circles stand for the AAHNC results from a previous work of Fu<sup>20</sup>.

### III. RESULTS AND DISCUSSIONS

The viscosities are calculated employing RWSP-VM, including a series of metal elements from low-Z to high-Z (Be, Al, Fe and U). One of the most significant parameters is the ionization of the metals, which affects the accuracy of viscosity. Hence, this should be discussed in details firstly. Followed are the viscosities of the four typical metals estimated from RWSP-VM, compared with the ones from different methods, respectively.

#### A. The Average Ionization

There are several methods to calculate  $\bar{Z}$ , such as Saha model, Thomas-Fermi (TF) model<sup>17</sup>, density functional theory molecular dynamics (DFT-MD)<sup>18,19</sup>, path integral Monte Carlo (PIMC)<sup>18</sup>, AAHNC<sup>20</sup>, and Hartree-Fock-Slater (HFS) method<sup>21</sup>. Here, we calculate  $\bar{Z}$  employing methods of TF (for Al, Fe, U and Be), HFS (for Al, Fe, U and Be), AAHNC (for Fe and Be) and Saha (for Al and Be). We use lowering ionization approximation from Ref. 22 in Saha model.

We analyze comprehensively the ionization from several methods and decide to use TF model to calculate  $\bar{Z}$  in our RWSP-VM unless otherwise specified according to the analysis below. Fig. 2 shows the calculated  $\bar{Z}$  of different methods, taking Al as an example. First, we compare  $\bar{Z}$  of Saha and TF models with  $\bar{Z}$  of Driver's methods<sup>18</sup> for  $T < 1000 \text{ eV}$ . The formers deviate from the latter within 16.6% (Saha-Driver) and 14.4% (TF-Driver). Similarly, comparing with AAHNC, the deviations of  $\bar{Z}$  are within 16.4% (Saha-AAHNC) and 6.3% (TF-AAHNC). Moreover, TF agrees better with HFS than Saha does from about 2 eV to 500 eV. In

general,  $\bar{Z}$  of TF model is more accurate than  $\bar{Z}$  of Saha model for  $T < 1000 \text{ eV}$ . The differences among these methods may be caused by several reasons, as noted by Driver et al.<sup>18</sup>. For example, at high temperature, the hybridization of the atomic orbitals is large enough that it is difficult to separate free and bound electrons, resulting in the difficulty to define  $\bar{Z}$  rigorously. Therefore, different methods may result in discrepancies due to their particular definitions of  $\bar{Z}$ . According to the above analysis, it indicates that TF is better than Saha in general.

Similarly, the average ionizations of Fe, U and Be at different densities are shown in Appendix. For Fe and U, TF is better. While it is the case of Be, Saha is better for lower density and TF is better for higher density. The influence of  $\bar{Z}$  calculated from Saha and TF for Be will be discussed in detail later.

When  $\bar{Z}$  is prepared, the viscosities could be easily calculated by RWSP-VM. The medium-Z metals are investigated usually, while the low-Z and high-Z metals are relatively seldom investigated. Therefore, we calculate and analyze the results in the order of medium-Z, high-Z and low-Z, employing Al, Fe, U and Be as examples. In order to validate RWSP-VM, in addition to comparing with the data of different methods, we also calculate the viscosities of Fe and Be employing LMD and CMD for comparisons in this work.

#### B. RWSP-VM for Al

Aluminum (Al) is a practical and fundamental metal and its viscosity is often helpful in warm dense matter applications, where RWSP-VM might agree better with CMD rather than LMD. Fig. 3 shows the viscosities of Al at the temperatures from about 2 eV to 1000 eV and at the densities of  $2.7 \text{ g/cm}^3$ ,  $8.1 \text{ g/cm}^3$  and  $27 \text{ g/cm}^3$ . In particular, solid curves stand for RWSP-VM results. It indicates that the viscosity increases with the increasing temperature and with the increasing density.

However, when the temperature is low enough, RWSP-VM is not suitable, showing that the viscosity still increases as the temperature increases. Actually, the fact is opposite according to our previous work<sup>23</sup>. Because the Debye length is so small ( $\lambda_D < 0.1a_{ws}$ ) that the Coulomb potential discussed in RWSP-VM is not the only interatomic interaction, and other interactions play more important roles. Here,  $a_{ws} = (\frac{3}{4\pi n})^{(1/3)}$  is the Wigner-Seitz radius of the ion. Therefore, we use the temperature  $T_{\text{lower}}$  at which  $\lambda_D(T_{\text{lower}}) = 0.1a_{ws}$  to cut off the viscosity curve, as shown with gray dashed lines. In other words, RWSP-VM is suitable for  $T > T_{\text{lower}}$ .

Besides, we also notice that the viscosity of RWSP-VM starts to decrease with the increasing temperature larger than the order of  $10^3 \text{ eV}$ , which is not correct compared with the results of Ref. 13. The reason is that “introducing a truncated range in the impact parameter is not equivalent to truncating the range of the

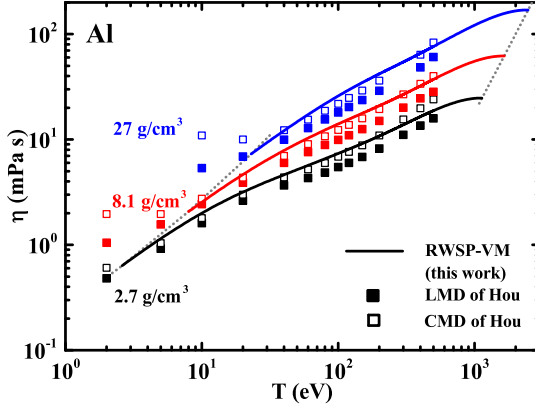


FIG. 3. Shear viscosity of Al. Solid lines stand for RWSP-VM results. Filled and open squares stand for LMD and CMD data from a previous work of Hou<sup>11</sup>, respectively. Black, red and blue stand for densities of  $2.7 \text{ g/cm}^3$ ,  $8.1 \text{ g/cm}^3$  and  $27 \text{ g/cm}^3$ , respectively. Gray dot lines stand for the lower (left) and upper (right) limits of temperatures.

Coulomb interaction”<sup>24</sup>. When the temperature is high enough, the Debye shielding effect is reduced and multi-body collisions become significant so that the quantity  $\langle(\Delta v_y)^2\rangle$  is underestimated due to Assumption 1. Here, we estimate the upper limit of temperature as  $T_{\text{upper}}$  at which  $\lambda_D(T_{\text{upper}}) = 0.5a_{ws}$ . In other words, RWSP-VM is suitable for  $T < T_{\text{upper}}$ .

Now we compare RWSP-VM with LMD and CMD<sup>11</sup> in the above range, the average ionization of which varies from 3 to 13. The values of RWSP-VM deviate from those of LMD and CMD within 46.4% and 21.6%, respectively. This indicates that RWSP-VM agrees better with CMD rather than LMD.

### C. RWSP-VM for Fe

Iron (Fe) is an important metal when investigating the core of terrestrial planets<sup>25–27</sup>. Since Fe is belong to medium-Z element, which behaves similarly to Al, RWSP-VM also illustrates good agreement with different methods below, e.g., agrees well with CMD rather than LMD. Fig. 4 shows the viscosities of Fe. Here, Daligault et al.<sup>13</sup> employ TFMD simulations, and Sun et al.<sup>28</sup> employ both OFMD and SRR simulations. The viscosities increase with increasing temperatures and increase with increasing densities. It indicates that RWSP-VM agrees well with the MD simulations in general, i.e., with TFMD and SRR. We notice that at lower densities (e.g.,  $4 \text{ g/cm}^3$  and  $7.9 \text{ g/cm}^3$ ), the viscosity of RWSP-VM is a bit larger than that of OFMD. But the results of RWSP-VM and SRR agree better with each other. Especially, the values of RWSP-VM deviate from those of OFMD and SRR from 0.51% to 46.1% and from 0.17% to 19.6%, respectively. This

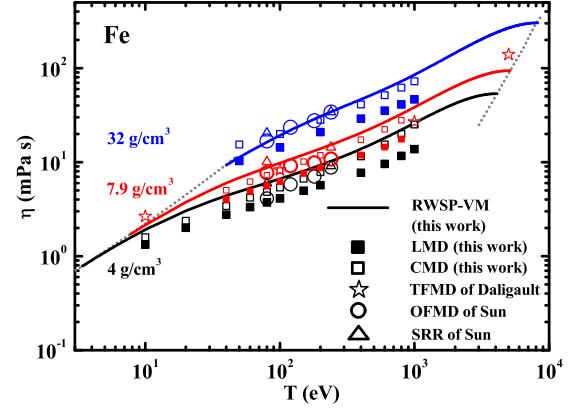


FIG. 4. Shear viscosity of Fe. Stars, circles and triangles stand for the results of TFMD<sup>13</sup>, OFMD and SRR<sup>28</sup>, respectively. Black, red and blue stand for densities of  $4 \text{ g/cm}^3$ ,  $7.9 \text{ g/cm}^3$  and  $32 \text{ g/cm}^3$ , respectively. Other legends are the same as Fig. 3. Notice that red stars correspond to the density of  $7.87 \text{ g/cm}^3$  for TFMD.

is because OFMD based on TF approximation is not suitable at low temperatures and densities, while SRR is more accurate due to the utilizing of the Yukawa model and the corresponding repulsion potential. The latter is similar to the shielding Coulomb potential used in this work. Furthermore, the LMD and CMD results are also shown for comparisons, which indicates that RWSP-VM agrees better with CMD rather than LMD. Here, the lower and upper limits of temperatures are still suitable for Fe.

### D. RWSP-VM for U

Uranium (U) is often used as the material for planar and hohlraum targets in the ignition experiments. Here, at higher densities RWSP-VM agrees better with LMD, while at lower densities RWSP-VM agrees better with CMD. Fig. 5 shows the viscosities of U. The viscosities increase with the increasing temperatures and densities. At the density of  $1.893 \text{ g/cm}^3$ , RWSP-VM agrees better with CMD rather than LMD. Especially, the values of RWSP-VM deviate from those of LMD and CMD from 35.9% to 147% and from 1.0% to 23.4%, respectively. While at the densities of  $18.93 \text{ g/cm}^3$  and  $94.65 \text{ g/cm}^3$ , RWSP-VM agrees better with LMD rather than CMD except for the few data at the highest temperatures. Especially, the values of RWSP-VM deviate from those of LMD and CMD from 1.7% to 20.4% and from 3.0% to 47.8%, respectively (except for the few data at highest temperatures). This phenomenon may be explained that “electron–ion dynamic collisions (introduced by LMD) increase the effective collision cross section and weaken the interaction between ions.”<sup>29</sup> This results in the fact that at higher densities, the Debye shielding effect, which

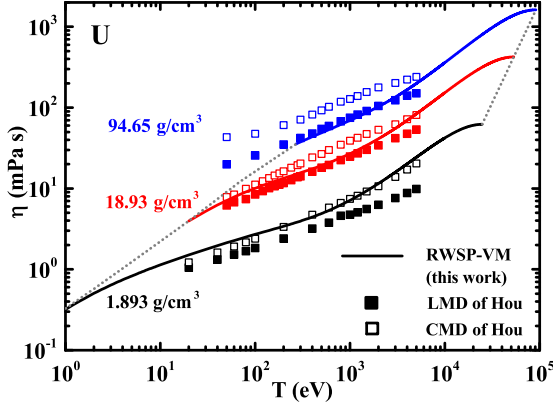


FIG. 5. Shear viscosity of U. Legends are the same as Fig. 3. LMD and CMD data are from a previous work of Hou<sup>29</sup>. Black, red and blue stand for densities of  $1.893 \text{ g/cm}^3$ ,  $18.93 \text{ g/cm}^3$  and  $94.65 \text{ g/cm}^3$ , respectively.

plays an important role in RWSP-VM, weakens the interaction between ions, corresponding to the case of LMD.

### E. RWSP-VM for Be

Beryllium (Be) plays an important role as an ablator in ICF<sup>30</sup>. Here, RWSP-VM agrees well with CMD and QMD rather than LMD, meanwhile, TF is better for higher density and Saha is better for lower density when estimating  $\bar{Z}$ . Fig. 6 shows the shear viscosity of Be. C. Wang et al.<sup>31</sup> employ QMD at the density of  $5 \text{ g/cm}^3$  and we employ LMD and CMD at the densities of  $1.85 \text{ g/cm}^3$ ,  $5.0 \text{ g/cm}^3$  and  $25 \text{ g/cm}^3$ . For the data of QMD ( $5 \text{ g/cm}^3$ ) and CMD ( $25 \text{ g/cm}^3$ ), the viscosities decrease firstly and then increase with the increasing temperatures. Because for these two cases the corresponding temperature ranges are from low to warm, where there is a competition relation between the kinetic and potential components of the particles at this range of temperature. Both components contribute to the viscosities. When the temperature is low, the kinetic one is negligible compared with the potential one, resulting in the decrease of viscosities due to decrease of the potential with the increasing temperature. When the temperature continues to increase, the kinetic one is no longer negligible, resulting in the increase of viscosities due to the increase of the kinetic one with the increasing temperature. This phenomenon has been illustrated in Ref. 32 and our previous work<sup>23</sup>. In warm dense range, the viscosities increase with increasing temperatures.

Here, we consider both TF and Saha models to calculate the average ionization (shown in Fig. A3) for comparison. We notice that the viscosities of RWSP-VM employing TF do not agree well with CMD and LMD at the condition of  $1.85 \text{ g/cm}^3$  and  $3 \text{ eV}$ , and the ones of

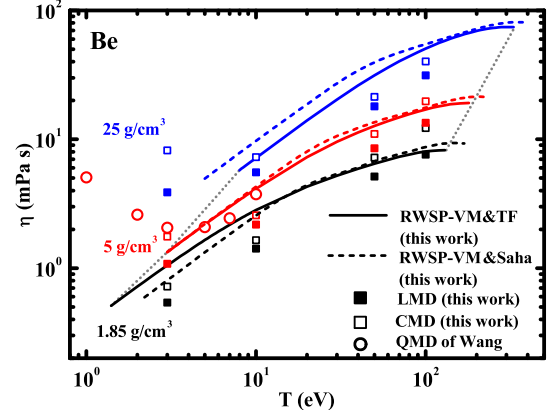


FIG. 6. Shear viscosity of Be. Solid and dashed lines stand for RWSP-VM results employing TF and Saha, respectively. Filled and open squares stand for LMD and CMD results, respectively. Open circles stand for QMD data from C. Wang<sup>31</sup>. Black, red and blue stand for densities of  $1.85 \text{ g/cm}^3$ ,  $5 \text{ g/cm}^3$  and  $25 \text{ g/cm}^3$ , respectively. Gray dot lines stand for the lower (left) and upper (right) limits of temperatures (only RWSP-VM employing TF is available here for clarify).

Saha also do not agree well with them at the condition of  $25 \text{ g/cm}^3$ . This is because for low ( $1.85 \text{ g/cm}^3$ ) and high ( $25 \text{ g/cm}^3$ ) densities,  $\bar{Z}$  of TF and Saha differs a lot, which influences the viscosities of RWSP-VM. Especially, at lower temperatures ( $3 \text{ eV}$ ),  $\bar{Z}$  of TF at  $1.85 \text{ g/cm}^3$  and  $\bar{Z}$  of Saha at  $25 \text{ g/cm}^3$  are underestimated, resulting in the inaccuracy of RWSP-VM employing TF ( $1.85 \text{ g/cm}^3$ ) and Saha ( $25 \text{ g/cm}^3$ ) for the corresponding cases. At the density of  $5 \text{ g/cm}^3$ , there are fewer differences of  $\bar{Z}$  between TF and Saha, resulting in the agreement in the viscosities between them. Therefore, at lower density ( $1.85 \text{ g/cm}^3$ ), the utilization of Saha is better, and at higher densities ( $5 \text{ g/cm}^3$  and  $25 \text{ g/cm}^3$ ), TF is better. This corresponding is used for the comparisons below. Especially, the viscosities of RWSP-VM deviate from the ones of CMD from  $6.3\%$  to  $28.9\%$  at  $1.85 \text{ g/cm}^3$  and  $5 \text{ g/cm}^3$  except for the temperature at  $10 \text{ eV}$ . The deviation between RWSP-VM and CMD is from  $1.2\%$  to  $50.0\%$  at  $25 \text{ g/cm}^3$  and the one between RWSP-VM and QMD is from  $4.7\%$  to  $35.2\%$ . In general, the viscosities of RWSP-VM agree well with CMD and QMD under corresponding conditions. Because Be is a low-Z element, the ionization is low enough (less than 4), which weakens the influence of electrons. This is the reason why we prefer CMD rather than LMD for comparison. It is the same reason for Al.

The characteristics of RWSP-VM are its universality, accuracy and high efficiency. The reasons are mainly summarized here. First, this model is based on the “random-walk”, “ion gas” and “shielding-potential” assumptions, which describe the physical pictures of warm dense metals. Accordingly, the different kinds of metal ions behave similarly in warm dense state. Second,

the “shielding potential” is treated as the Coulomb potential employing a cut-off distance described with the Debye length, which is a good approximation for warm dense metals. Third, the “binary collision” is the dominant event for the dynamic process in warm dense regime, and this assumption makes it simple enough to obtain a simple formula.

#### IV. CONCLUSIONS

The statistics of random-walk ions and the Debye shielding effect are taken in RWSP-VM. Based on RWSP-VM, we accurately estimate the shear viscosities of a series of metal elements in warm dense state in a flash. In general, the methods of MD simulations such as QMD etc. cost several days to simulate for one state point, while our model obtains one within a second. Also, based on RWSP-VM, the shear viscosities of arbitrary element can be obtained, which should be applied to numerous areas and really important in warm and dense physics.

#### ACKNOWLEDGMENT

We thank Shuaichuang Wang and Cong Wang for helpful discussions. This work was financially supported by Science Challenge Project, No. TZ2016001 and the Foundation of LCP. Hou was supported by Science Challenge Project, No. TZ2018005 and National Natural Science Foundation of China under No. 11974424.

#### APPENDIX: AVERAGE IONIZATION

The average ionizations of Fe, U and Be at different densities are shown in Fig. A1, A2 and A3, respectively.

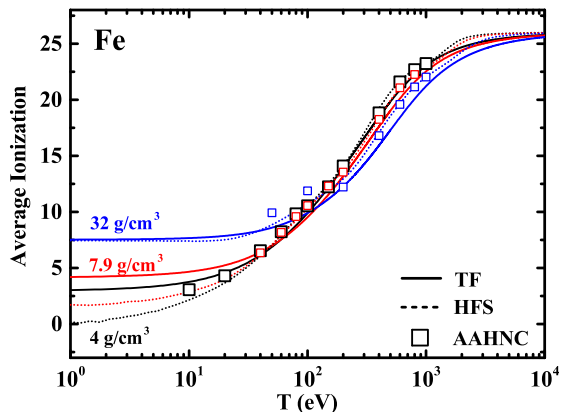


FIG. A1. Average ionization  $\bar{Z}$  of Fe at the densities of  $4 \text{ g/cm}^3$  (black),  $7.9 \text{ g/cm}^3$  (red) and  $32 \text{ g/cm}^3$  (blue). Solid and dot lines stand for the results of TF and HFS models, respectively. Open squares stand for the ones of AAHNC.

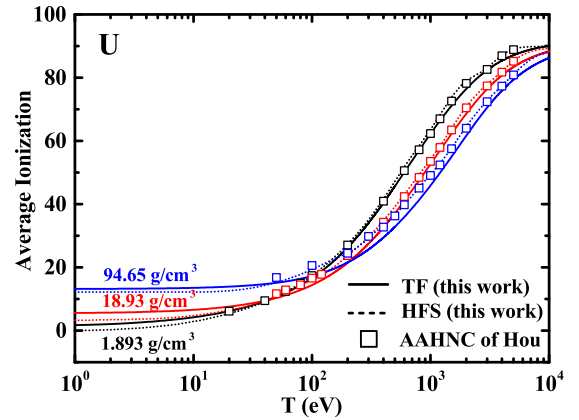


FIG. A2. Average ionization  $\bar{Z}$  of U at the densities of  $1.893 \text{ g/cm}^3$  (black),  $18.93 \text{ g/cm}^3$  (red) and  $94.65 \text{ g/cm}^3$  (blue). Legends are the same as Fig. A1. Data of AAHNC are from a previous work of Hou<sup>29</sup>.

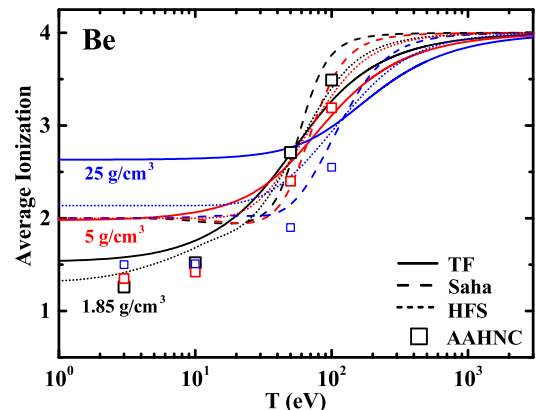


FIG. A3. Average ionization  $\bar{Z}$  of Be at the density of  $1.85 \text{ g/cm}^3$  (black),  $5 \text{ g/cm}^3$  (red) and  $25 \text{ g/cm}^3$  (blue). Solid, dashed and dot lines stand for the results of TF, Saha and HFS models, respectively. Open squares stand for the one of AAHNC.

The differences of the viscosities among different methods are given in the main text, while the ones of  $\bar{Z}$  are analyzed below. In Fig. A1, TF, HFS and AAHNC agree well with each other, except for lower temperatures. In Fig. A2, the relative differences among TF, HFS and AAHNC are small enough due to the large atomic number of U. As a result, for the average ionizations of Fe and U, TF is an applicable model, which is the same as Al. However, it is not that applicable for Be. In Fig. A3, at the density of  $1.85 \text{ g/cm}^3$ , compared with HFS and AAHNC, TF behaves better than Saha, especially at lower temperatures ( $T < 30 \text{ eV}$ ). While at  $5 \text{ g/cm}^3$ , TF and Saha agree well with HFS and AAHNC except for lower temperatures. Moreover, at  $25 \text{ g/cm}^3$ , compared with HFS, Saha behaves better than TF, while compared with AAHNC, none of the other three agree

well. The relatively large errors may originate from the low atomic number of Be. Hence, for different densities of Be, different methods for  $\overline{Z}$  should be employed, i.e., TF for lower densities and Saha for higher densities. This is implemented to calculate the viscosities of Be in the main text.

## REFERENCES

- <sup>1</sup>J. Lindl, O. Landen, J. Edwards, and E. Moses, "Review of the national ignition campaign 2009-2012," *Physics of Plasmas* **21**, 020501 (2014).
- <sup>2</sup>A. Y. Wong, R. W. Motley, and N. D'Angelo, "Landau damping of ion acoustic waves in highly ionized plasmas," *Physical Review* **133**, A436–A442 (1964).
- <sup>3</sup>O. Durand, S. Jaouen, L. Soulard, O. Heuzé, and L. Colombe, "Comparative simulations of microjetting using atomistic and continuous approaches in the presence of viscosity and surface tension," *Journal of Applied Physics* **122**, 135107 (2017).
- <sup>4</sup>J. Dai, Y. Hou, D. Kang, H. Sun, J. Wu, and J. Yuan, "Structure, equation of state, diffusion and viscosity of warm dense fe under the conditions of a giant planet core," *New Journal of Physics* **15**, 045003 (2013).
- <sup>5</sup>G. H. Miller and T. J. Ahrens, "Shock-wave viscosity measurement," *Reviews of Modern Physics* **63**, 919–948 (1991).
- <sup>6</sup>X.-J. Ma, B.-B. Hao, H.-X. Ma, and F.-S. Liu, "Shear viscosity of aluminum studied by shock compression considering elastoplastic effects," *Chinese Physics B* **23**, 096204 (2014).
- <sup>7</sup>D. Alfé and M. J. Gillan, "First-principles calculation of transport coefficients," *Physical Review Letters* **81**, 5161–5164 (1998).
- <sup>8</sup>M. P. Allen and D. J. Tildesley, *Computer simulation of liquids* (Clarendon Press, 1989).
- <sup>9</sup>S. Wang and H. Liu, "Transport properties of liquid aluminum at high pressure from quantum molecular dynamics simulations," in *Computational Science and Its Applications – ICCSA 2017*, edited by O. Gervasi, B. Murgante, S. Misra, G. Borruso, C. M. Torre, A. M. A. C. Rocha, D. Taniar, B. O. Apduhan, E. Stankova, and A. Cuzzocrea (Springer International Publishing) pp. 787–795.
- <sup>10</sup>S. Wang, G. Zhang, B. Sun, H. Song, M. Tian, J. Fang, and H. Liu, "Quantum molecular dynamics simulations of transport properties in liquid plutonium," *Chinese Journal of Computational Physics* **36**, 253–258 (2019).
- <sup>11</sup>Y. Hou, Y. Fu, R. Bredow, D. Kang, R. Redmer, and J. Yuan, "Average-atom model for two-temperature states and ionic transport properties of aluminum in the warm dense matter regime," *High Energy Density Physics* **22**, 21–26 (2017).
- <sup>12</sup>C. E. Starrett, J. Daligault, and D. Saumon, "Pseudoatom molecular dynamics," *Physical Review E* **91**, 013104 (2015).
- <sup>13</sup>J. Daligault, S. D. Baalrud, C. E. Starrett, D. Saumon, and T. Sjostrom, "Ionic transport coefficients of dense plasmas without molecular dynamics," *Physical Review Letters* **116**, 075002 (2016).
- <sup>14</sup>J. Daligault, K. Ø. Rasmussen, and S. D. Baalrud, "Determination of the shear viscosity of the one-component plasma," *Physical Review E* **90**, 033105 (2014).
- <sup>15</sup>M. S. Murillo, "Viscosity estimates of liquid metals and warm dense matter using the yukawa reference system," *High Energy Density Physics* **4**, 49–57 (2008).
- <sup>16</sup>N. v. Kampen, *Stochastic Processes in Physics and Chemistry, Third edition* (North-Holland, New York, 1981).
- <sup>17</sup>L. H. Thomas, "The calculation of atomic fields," *Mathematical Proceedings of the Cambridge Philosophical Society* **23**, 542–548 (1927).
- <sup>18</sup>K. P. Driver, F. Soubiran, and B. Militzer, "Path integral monte carlo simulations of warm dense aluminum," *Physical Review E* **97**, 063207 (2018).
- <sup>19</sup>M. Bethkenhagen, B. B. L. Witte, M. Schörner, G. Röpke, T. Döppner, D. Kraus, S. H. Glenzer, P. A. Sterne, and R. Redmer, "Carbon ionization at gigabar pressures: An ab initio perspective on astrophysical high-density plasmas," *Physical Review Research* **2**, 023260 (2020).
- <sup>20</sup>Y. Fu, Y. Hou, D. Kang, C. Gao, F. Jin, and J. Yuan, "Multi-charge-state molecular dynamics and self-diffusion coefficient in the warm dense matter regime," *Physics of Plasmas* **25**, 012701 (2018).
- <sup>21</sup>X.-J. Meng, Y.-S. Sun, and S.-C. Li, "Calculation of atomic average degree of ionization," *Acta Physica Sinica* **43**, 345–350 (1994).
- <sup>22</sup>Z. Fu, W. Quan, W. Zhang, Z. Li, J. Zheng, Y. Gu, and Q. Chen, "Equation of state and transport properties of warm dense aluminum by ab initio and chemical model simulations," *Physics of Plasmas* **24**, 013303 (2017).
- <sup>23</sup>Y. Cheng, H. Wang, S. Wang, X. Gao, Q. Li, J. Fang, H. Song, W. Chu, G. Zhang, H. Song, and H. Liu, "Deep-learning potential method to simulate shear viscosity of liquid aluminum at high temperature and high pressure by molecular dynamics," *AIP Advances* **11**, 015043 (2021).
- <sup>24</sup>L. G. Stanton and M. S. Murillo, "Ionic transport in high-energy-density matter," *Physical Review E* **93**, 043203 (2016).
- <sup>25</sup>T. Lay, J. Hernlund, and B. A. Buffett, "Coremantle boundary heat flow," *Nature Geoscience* **1**, 25–32 (2008).
- <sup>26</sup>M. Pozzo, C. Davies, D. Gubbins, and D. Alfé, "Thermal and electrical conductivity of iron at earth's core conditions," *Nature* **485**, 355–358 (2012).
- <sup>27</sup>S. Anzellini, A. Dewaele, M. Mezouar, P. Loubeyre, and G. Morard, "Melting of iron at earth's inner core boundary based on fast x-ray diffraction," *Science* **340**, 464–466 (2013).
- <sup>28</sup>H. Sun, D. Kang, Y. Hou, and J. Dai, "Transport properties of warm and hot dense iron from orbital free and corrected yukawa potential molecular dynamics," *Matter and Radiation at Extremes* **2**, 287–295 (2017).
- <sup>29</sup>Y. Hou, Y. Jin, P. Zhang, D. Kang, C. Gao, R. Redmer, and J. Yuan, "Ionic self-diffusion coefficient and shear viscosity of high-z materials in the hot dense regime," *Matter and Radiation at Extremes* **6**, 026901 (2021).
- <sup>30</sup>J. D. Lindl, P. Amendt, R. L. Berger, S. G. Glendinning, S. H. Glenzer, S. W. Haan, R. L. Kauffman, O. L. Landen, and L. J. Suter, "The physics basis for ignition using indirect-drive targets on the national ignition facility," *Physics of Plasmas* **11**, 339–491 (2004).
- <sup>31</sup>C. Wang, Y. Long, M.-F. Tian, X.-T. He, and P. Zhang, "Equations of state and transport properties of warm dense beryllium: A quantum molecular dynamics study," *Phys. Rev. E* **87**, 043105 (2013).
- <sup>32</sup>V. G. Postovalov, E. P. Romanov, V. P. Kondrat'ev, and V. I. Kononenko, "Theory of transport in liquid metals: Calculation of dynamic viscosity," *High Temperature* **41**, 762–770 (2003).